TISSUE ENGINEERING: Part A
Volume 19, Numbers 7 and 8, 2013

DOI: 10.1089/ten.tea.2012.0309

Impact of Electrospun Conduit Fiber Diameter and Enclosing Pouch Pore Size on Vascular Constructs Grown Within Rat Peritoneal Cavities

Chris A. Bashur, PhD,[1] Matthew J. Eagleton, MD,[2] and Anand Ramamurthi, PhD[1]

The generation of vascular grafts by recruiting autologous cells within the peritoneal cavity has shown promise. However, the microenvironment affects cell differentiation and elastic matrix production. Therefore, this study determined the impact of systematic changes in the average fiber diameter of electrospun poly(ε-caprolactone) conduits, and the pore size of pouches used to enclose the conduits, on recruited cells. After 2 weeks in the peritoneal cavity, fibrous capsules formed containing macrophages, α-smooth muscle actin $(\alpha\text{-SMA})^+$ and $SM22\alpha^+$ myofibroblastic or smooth muscle like-cells, and what appeared to be mesothelial cells on the outer surfaces. These cells infiltrated and deposited matrix (e.g., collagen, hyaluoronan, and limited elastin) within conduit walls. Constructs enclosed within the largest pore pouches exhibited significantly better tissue generation responses (e.g., better cell infiltration, elongation, and matrix deposition). Additionally, the healing response was impacted by the conduit average fiber diameter, and consequently, the effective pore diameter, with the largest diameter fibers promoting the most positive healing response (e.g., greater total cellularity, extracellular matrix deposition, and $\alpha\text{-SMA}^+$ cells). Six weeks post-intra-aortal grafting, constructs were occluded, but significant remodeling also occurred in the arterial microenvironment. Overall, these results demonstrate the importance of microenvironmental cues on recruited peritoneal cells and the necessity of developing strategies to further improve elastic matrix synthesis.

Introduction

Coronary heart disease accounts for approximately one in every five deaths in the United States. Occlusion of small-diameter coronary vessels (i.e., those <6 mm) is a primary symptom of the disease.[1,2] Autologous vessels (e.g., saphenous veins) are the gold standard for bypass grafting in patients with blocked arteries, but are unavailable in $>30\%$ of affected patients due to systemic vascular disease.[3] Synthetic vascular prostheses—for example, expanded poly (tetrafluoroethylene) (ePTFE)—have been used as alternatives, but they trigger a strong inflammatory response, tend to thrombose, and exhibit compliance mismatches with the native vascular tissue.[4] Activation of smooth muscle cells (SMCs) can also lead to overexpression of proteolytic enzymes, resulting in aneurysmal expansion of the graft.[5] Thus, alternative strategies, such as the use of self-repairing, tissue-engineered vascular grafts, are needed to circumvent these challenges.

Only a limited number of tissue-engineered vascular grafts have shown promise in clinical trials to date.[6–8] Significant concerns with these grafts include the extended time frame and high costs for *in vitro* manipulation of seeded cells. Additionally, long-term patency of these grafts can be compromised by the poor cellular synthesis of elastin precursors and their limited ability to assemble them into elastic matrix superstructures typical of native vessels.[9,10] The elastic matrix provides the mechanics required for the vascular tissue and also regulates the SMC phenotype.[11] Most adult cell types inherently synthesize very limited amounts of elastin.[12] Therefore, strategies have been developed to improve elastic matrix production and maturation, including by growth factor stimulation—for example, tetramers of hyaluronan (HA) and transforming growth factor-β1.[13,14] While some of these strategies have shown promise, more mature and directionally aligned elastic fibers are still required to create functional small-diameter vascular grafts. Since fetal and neonatal cell types produce significantly more elastin than adult cells,[15,16] we hypothesize that recruitment (e.g., within the peritoneal cavity)[17,18] of stem or progenitor cell populations to implanted scaffolds, and their subsequent differentiation, may improve elastic matrix production. These recruited peritoneal cells may circumvent both the poor elastogenicity of differentiated adult cell types and the need to process them *in vitro*.

Departments of [1]Biomedical Engineering and [2]Vascular Surgery, Cleveland Clinic, Cleveland, Ohio.

Work by Campbell *et al*.[17] first demonstrated the possibility of using the peritoneal cavity as a substitute bioreactor to generate autologous, tissue-engineered constructs without *in vitro* manipulations. In a series of studies, they demonstrated that tubular tissue constructs, containing macrophages, mesothelial cells, and myofibroblastic cells, could be produced around a silicone tube inserted into the peritoneal cavity for either 2 or 3 weeks.[17,19–22] However, limited elastin (i.e., 9% of native aortae) was found in rats and none was found in dogs. Most of these grafts remained patent up to 6.5 months after arterial grafting in rats, rabbits, and dogs, although longer time periods were not tested.[17,19] Another concern is the variable responses that have been found in the peritoneal cavity. For example, Song *et al.* employed a similar method in mice and found that the silicone tube required 8 weeks in the peritoneal cavity to generate sufficient tissue for grafting, among other differences.[18] Finally, although Song *et al.* did not find that their inserted tubes adhered to the surrounding peritoneal tissue,[18] others have shown that adhesion formation is a concern that must be addressed.[23] Therefore, improved elastic matrix production is necessary in these constructs, and focused study into the impact of different microenvironmental cues on the peritoneal cell phenotype and matrix production is required.

Surface topography of a scaffold is one microenvironmental factor that can potentially impact phenotype and patterns of extracellular matrix (ECM) deposition by recruited peritoneal cells. Topopgraphic features of scaffolds (e.g., electrospun meshes) can guide the alignment of seeded cells and their deposited ECM,[13,24] unlike the smooth-surface silicone tubes tested previously.[17] In addition, differences in the topographical features (e.g., fiber diameter) can also impact the effective pore dimensions of the scaffold.[25] The pore diameter is a concern for electrospun meshes, especially those with smaller average fiber diameters, where the pores may not be large enough to enable cell infiltration and cellular deposition of ECM within.[26] An additional consideration is that a combination of the fiber diameter and, correspondingly, the scaffold pore dimensions may impact the recruited peritoneal cell phenotype and matrix production. For example, Madden *et al.* found that the macrophage phenotype (i.e., proinflammatory M1 vs. prohealing M2) varies when cultured on a scaffold incorporating different-sized micro-spherical pores.[27] Therefore, understanding the impact of scaffold topography and fiber diameter/pore size on recruited cells is necessary for developing an autologous vascular construct.

In this study, we specifically determined the peritoneal cell ECM production in response to electrospun poly(ε-caprolactone) (PCL) conduits and the role of fiber diameter, which intrinsically impacts pore dimensions, on the recruited peritoneal cell phenotype, differentiation, and matrix synthesis. These conduits were enclosed within relatively non-adherent, porous PTFE pouches to prevent tissue adhesions. The pouches incorporated one of two different-sized pores. Our study investigated how pouch pore sizes impact the extent of cell recruitment, phenotype, and matrix production. After 2 weeks in the peritoneal cavity, the tissue-containing constructs were removed and either grafted intra-aortally to determine patency or analyzed for cell infiltration, cell phenotype, and matrix composition.

Materials and Methods

Materials

All disposables, chemicals, and biological supplies were purchased from VWR (West Chester, PA) unless specified otherwise. Antibodies were purchased from Abcam (Cambridge, MA), unless specified otherwise. PCL (inherent viscosity 1.0–1.3 dL/g in chloroform) was purchased from Lactel Absorbable Polymers (Pelham, AL).

Electrospun conduits

Electrospinning was performed using 14.5%, 17%, and 22% w/v PCL in 90% v/v chloroform and 10% dimethylformamide to form fibrous meshes with different average diameters. PCL was selected since PCL meshes have had tensile strengths similar to human coronary arteries.[13,28,29] Electrospinning was performed using a 22-gauge needle, 11-kV voltage gradient, 3-mL/h flow rate, and 15-cm throw distance. The fibers were electrospun for 25 min onto a 1.6-mm diameter aluminum rod. The rod was rotated slowly (i.e., 50–100 rpm) and moved laterally to maintain a consistent thickness throughout the circumference and length of the conduit. After electrospinning, the conduits were removed from the rod, cut into 1-cm-long sections, allowed to air-dry, and stored in a dessicator until use.

Conduit characterization

Fiber properties and ultrastructure. Diameters and degree of orientation of fibers were determined from scanning electron microscopy (SEM) images. For SEM, the electrospun conduits were mounted onto aluminum stubs, sputter-coated, and then imaged using a JEOL JSM 5310 (Peabody, MA) operating at 15 kV with a working distance of 10 mm. Conduit wall thickness was measured from cross-sections with light microscopy using an Olympus IX51 microscope (Olympus Corp., Center Valley, PA). The resultant images were imported into ImagePro Plus software (Media Cybernetics, Bethesda, MD) for analysis. The degree of orientation was characterized by angular standard deviation (ASD), where a lower ASD indicates a mesh containing more aligned fibers.[30]

Mechanical testing. The tensile properties of electrospun conduits were determined using an Instron 5943 under physiological conditions—that is in phosphate-buffered saline (PBS) maintained at 37°C. The average fiber diameters of these conduits were similar to those intraperitoneally implanted for the other assays, although the conduits were electrospun from solutions with different concentrations of PCL (i.e., 14%, 17%, and 20% w/v). For mechanical testing, individual tube specimens were loaded between two parallel rods and extended, similar to the procedure described by Soffer *et al*.[31] The length of the conduits or constructs (i.e., gauge width during the test) was 5 mm and the gauge lengths were between 3.2 and 3.5 mm for the different conditions (i.e., approximately, the luminal circumference divided by 2). The samples were subjected to 10 precycles (5% maximum strain at 10 mm/min) before stretching to failure at 10 mm/min. Modulus was calculated from the linear region of the stress–strain curve (i.e., the section

spanning a 4% strain range that had the highest modulus). This range was present after the initial, limited toe region. Yield strain and yield stress were also calculated.

Intraperitoneal implantation of electrospun scaffolds

For *in vivo* intraperitoneal implantation, 3–4 replicate conduits fabricated using the same electrospinning conditions, were enclosed within PTFE pouches with diamond-shaped pores (McMaster-Carr, Robbinsville, NJ). Pouches incorporating either of two different pore sizes were tested (i.e., 0.64×0.13 mm and 1.1×0.64 mm) to determine the impact on tissue growth around the enclosed conduits. ePTFE control conduits with a 2-mm luminal diameter were also included in the pouches as controls. The pouches and electrospun conduits were ethylene oxide sterilized before implantation.

Surgical implantation of sterilized pouches in the peritoneal cavities of 200–250 g male Sprague-Dawley rats (Charles River, Wilmington, MA) was performed in accordance with IACUC-mandated protocols. A ventral laparotomy was performed with the rat under isofluorane anesthesia and two pouches (i.e., one with small pores and the other with large pores, each containing conduits from the same electrospinning condition) were inserted into each rat. Constructs intended for mechanical testing were inserted individually without enclosure within a pouch. It was the results from this initial mechanics study that motivated the use of PTFE pouches to prevent adhesion of the peritoneal tissue to the electrospun conduits. The muscle and skin layers were closed with 4-0 Vicryl and Ethilon sutures, respectively (Ethicon, Somerville, NJ), and the animals were allowed to recover. In a replicate study, the pouches were hydrated with ethanol, and then saline before insertion, and the peritoneal cavity was flushed with saline before closing. In both studies, the pouches were removed after 2 weeks, and the conduits were either grafted into the infrarenal abdominal aorta of the same rats or processed for analysis.

Intra-aortal grafting of autologously grown tissue constructs

Following explantation from the peritoneal cavity, tissue constructs grown using 22% w/v PCL conduits were grafted into the infrarenal abdominal aorta. A ventral laparotomy was performed on the rats under isofluorane anesthesia, and then a 5–15-mm section of the aorta was dissected from the surrounding tissue and the vena cava. The aorta was clamped both above the graft site and just above the iliac bifurcation. An incision was made in the aorta and the ends were allowed to contract from the elastic recoil. Before grafting, the construct was cut to the appropriate length and soaked in the heparin sodium (1000 USP units/mL; APP Pharmaceuticals, Schaumburg, IL) for 5 min to reduce thrombus formation. The graft was sutured first at the distal anastomosis, followed by the proximal one. Four interrupted sutures (9-0 Nylon; Surgical Specialties Corp., Reading, PA) were placed at each anastomosis, and additional sutures were added as necessary. The distal clamp was released to allow the graft to fill with blood under low pressure, and then the proximal clamp was released to allow blood flow under full arterial pressure. After the determination of a pulse and the absence of leaking, the cavity was briefly flushed with warm saline. The peritoneal grafts were photographed with a stereomicroscope (Olympus SZ61, Center Valley, PA) equipped with a high-resolution CCD camera (Olympus Infinity 2) for diameter measurements before closing the cavity. After 6 weeks, the grafts were removed and prepared for sectioning.

Imaging and image analysis

Constructs were mounted in OCT (Tissue-Tek, Torrance, CA), and 8-μm cross- and longitudinal-sections were prepared. The sections were fixed in 4% w/v EM-grade formaldehyde (Polysciences, Inc., Warrington, PA) for 5 min, and then washed two times in PBS. Control ePTFE conduits were not imaged due to the negligible number of cells.

Histology. Histology was used to assess peritoneal cell recruitment, distribution, morphology (e.g., aspect ratio), and the structure and composition of their generated ECM. Tissue sections were stained with hematoxylin and eosin (Sigma, St Louis, MO) to visualize cell morphology and a general matrix ultrastructure. Modified Verhoff's Van Gieson staining (ScyTek Laboratories, Logan, UT) was performed according to the manufacturer's protocol to detect specific matrix components (e.g., elastin and collagen). An Oil Red O stain (ScyTek Laboratories) was used to detect the presence of lipid droplets, as are found in vascular foam cells (i.e., macrophage and/or SMC derivatives). Xylene was avoided during processing, since it dissolves the electrospun PCL fibers. Sections were cover-slipped using a mounting medium with limonene as the solvent (Electron Microscopy Sciences, Hatfield, PA), except for the Oil Red O stained samples that were mounted with an aqueous-based mount (Electron Microscopy Sciences).

Imunofluorescent labeling for cell phenotypic markers and ECM. Immunofluorescence was used to identify cell type-specific phenotypic markers expressed by peritoneal cells recruited to the electrospun conduits and to confirm components of the ECM generated by the recruited cells, similar to previous studies.[14] Briefly, the sections were permeabilized with 0.1% v/v Triton X-100 (VWR) for 10 min, and the cells were blocked with 5% v/v goat serum (PAA Laboratories, Inc., Dartmouth, MA). The cell phenotype was assessed with primary antibodies that detected markers of the SMC phenotype[32] (i.e., SM22α and α-smooth muscle actin [α-SMA]) and different macrophage phenotypes (i.e., CD68 as a general macrophage marker and CD80 for a proinflammatory M1 phenotype). The markers were visualized with secondary antibodies conjugated to Alexa 633 probes (Invitrogen, Grand Island, NY). The presence of matrix proteins was detected with primary antibodies against collagen type 1 and elastin. HA was detected with a biotinylated HA-binding protein (EMD Chemicals, Inc., San Diego, CA) and visualized with a streptavidin-conjugated Alexa 633 probe (Invitrogen). Cell nuclei were visualized with 4′,6-diamino-2-phenylindole dihydrochloride (DAPI) contained in the mounting medium (Vectashield, Vector Labs, CA). Imaging was performed on an Olympus IX51 microscope. The brightness and contrast were adjusted equally for all cases and for the immunofluorescent labeling control (i.e., no primary antibody). Nuclear morphology and cell infiltration

were quantitatively assessed from these images with ImagePro Plus® software using a custom script that creates areas of interest and measures the number of nuclei, nuclear area, and nuclear aspect ratio for both the fibrous capsule (i.e., the area outside of the electrospun fibers) and 50-μm sections throughout the thickness of the conduit wall. The morphology of cell nuclei has been shown to directly correlate to the morphology of the entire cell.[13,33] Nuclei were measured in this study instead of entire cells due to the limited ability to reliably outline individual cells in confluent culture. For aspect ratio, the ImagePro Plus software fits an ellipse to the outlined cell nuclei.

Transmission electron microscopy. Transmission electron microscopy (TEM) was performed on explanted tissue constructs to assess cellular features and the matrix ultrastructure. Samples were fixed in 4% w/v glutaradehyde in 0.2 M cacodylate buffer overnight at 25°C. Secondary fixation was performed with 1% w/v osmium tetroxide for 60 min at 4°C. Dehydration was performed with ethanol and propylene oxide. Samples were mounted and 1-μm longitudinal sections were prepared. The grids were also labeled with 1% w/v uranyl acetate to increase contrast. Images were taken with a Philips CS12/STEM (FEI Company, Hillsboro, OR).

Biochemical analysis

Cellularity. A DNA assay was performed on the peritoneal constructs to quantify cellularization after 2 weeks. The constructs were digested in 200 μL of 5 mg/mL proteinase-K (Invitrogen) in PBS for 12 h at 50°C. Afterward, the samples were sonicated (Branson Sonifier 150; Emerson Industrial Automation, Danbury, CT) for 1 min to lyse remaining cells and to release the DNA. An aliquot was removed for quantification of the protein content, with the remaining volume retained for DNA quantification with Hoechst 33258 dye. DNA was quantified with a fluorometric assay described previously by Labarca and Paigen.[34] Samples were diluted in a Pi buffer (50 mM $NaHCO_3$, 2 mM EDTA, and 0.02% w/v sodium azide; pH 7.4) during analysis. Cell densities were calculated based on the estimate of 6 pg of DNA/cell.

Assay for collagen content. A hydroxyproline (OH-Pro) assay was used to estimate the amounts of collagen deposited by peritoneal cells recruited to the implanted electrospun conduits. The sonicated aliquot from the previous section was further digested in 0.1 M sodium hydroxide (98°C, 1 h), and then hydrolyzed. As described previously,[35] 500 μL of 6 M HCL was added to 600 μL of the digestate, the sample was hydrolyzed (110°C, 16 h), and finally dried under a nitrogen stream at 37°C. Aliquots (20 μL) of the reconstituted residues were assayed with the OH-Pro assay, as described previously.[35,36] Collagen amounts were then calculated on the basis of the 13.2% w/w OH-Pro content of collagen, and normalized to the luminal area of the corresponding conduits.

Assay for elastin content. A Fastin® assay (Accurate Chemical and Scientific Corporation, Westbury, NY) was used to quantify the total amount of matrix elastin, as described previously.[35] Briefly, an aliquot from the protein samples after alkali treatment (see the previous section) was solubilized with 0.25 M oxalic acid (98°C, 1 h), and then assayed with the Fastin assay. The Fastin assay was performed as described in the manufacturer's protocol. The measured elastin protein amounts were normalized to the luminal area of the corresponding conduits.

Statistics

Results are presented as the mean ± standard deviation. A total of $n > 60$ fibers/condition (three images/condition) were used for SEM analysis of electrospun conduits, $n > 10$ measurements/condition were used to determine the conduit wall thickness, $n = 6$ samples/condition were used for tensile testing of constructs preinsertion, and $n = 3$ samples/condition for testing 2 weeks postinsertion, and $n = 7$ samples/condition were used for biochemical assays. Cell infiltration was determined with $n = 4$ images/condition. Observations from histological and immunofluorescent images were determined on $n = 2$ samples/condition (three images/sample). All studies were replicated using different rats and batches of electrospun meshes to ensure reproducibility. Statistical analysis was performed with SPSS software and statistical significance determined using one-way ANOVA with *post hoc* comparisons, using the Tukey method for a significance criterion of $p \leq 0.05$.

Results

Morphological characterization of electrospun conduits

Electrospun conduits containing fibers of different diameter ranges were generated and characterized with SEM (Fig. 1). For 14.5%, 17%, and 22% w/v PCL solutions, the average fiber diameters for the outer conduit surfaces were 0.62 ± 0.4, 1.4 ± 0.7, and 1.9 ± 0.8 μm, respectively (Table 1; all different with $p < 0.001$). A limited number of beads were observed in the 14.5% w/v PCL conduits (Fig. 1A, D). By setting an electrospinning time of 25 min, meshes were produced with average wall thicknesses between 400 and 500 μm. Although the target mandrel was rotated slowly, a limited degree of orientation was observed, with all ASDs greater than 40° (Table 2). The direction of orientation for the luminal surface varied depending on a polymer solution concentration, with conduits electrospun from 14.5% w/v PCL exhibiting a random orientation and conduits from 17% and 22% w/v PCL exhibiting orientation along the length of rod. Finally, the large fiber diameter, 22% w/v PCL conduits alone exhibited a significant decrease in the fiber diameter for the outer compared to the luminal surface (i.e., 2.9 ± 0.6 vs. 1.9 ± 0.8 μm, $p < 0.001$) and the average direction of orientation for the outer surface was shifted 85° (i.e., from along the length of the tube to around the circumference).

Impact of pouch pore size and electrospun fiber diameter on tissue generation

Impact on cell infiltration and capsule thickness. Free-floating pouches with enclosed electrospun conduits (Fig. 1G, H) were inserted into rat peritoneal cavities for 14 days. The surrounding peritoneal tissue was unable to penetrate the pouch pores, preventing adhesion to the electrospun conduits. However, significant tissue deposition was observed within the pouches, including around the conduits.

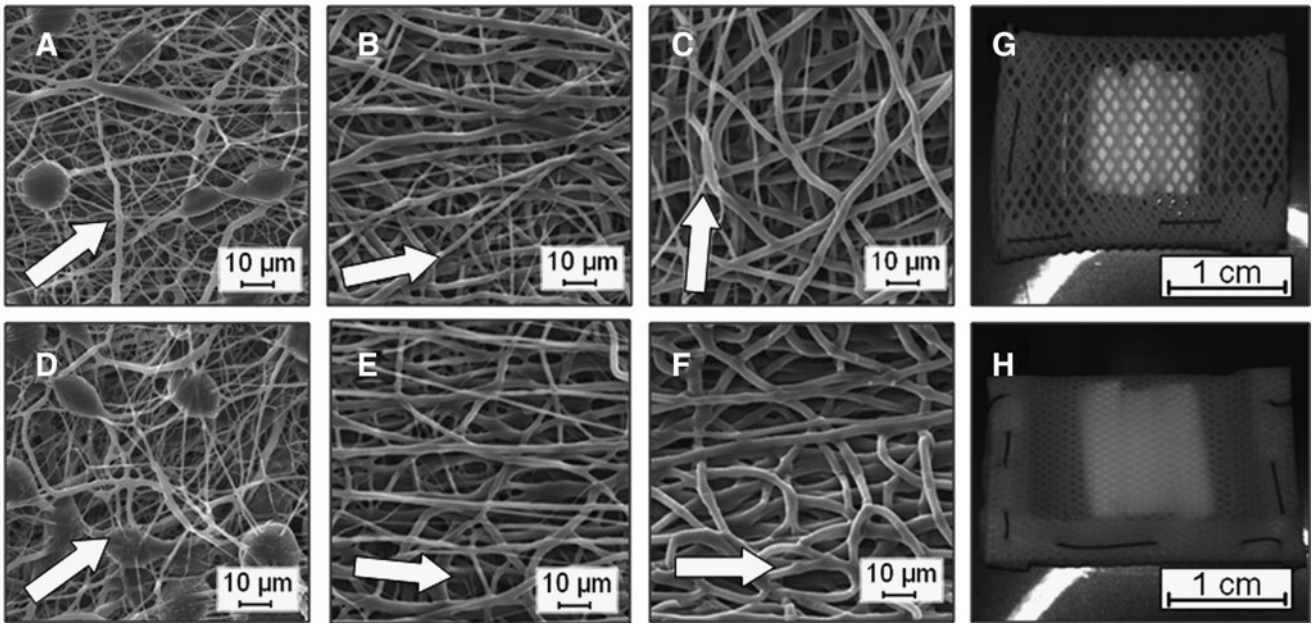

FIG. 1. Electrospun poly(ε-caprolactone) (PCL) conduits exhibit a range of average fiber diameters. Shown are scanning electron microscopy images of meshes electrospun from solutions containing 14.5% w/v **(A, D)**, 17% w/v **(B, E)**, and 22% w/v **(C, F)** of PCL. Images **(A–C)** are of the outer surface and images **(D–F)** are of the luminal surface of the conduits. An arrow indicates the average direction of fiber orientation. These constructs were included within poly(tetrafluoroethylene) (PTFE) pouches with either larger **(G)** or smaller **(H)** pores to allow peritoneal cells and fluid to penetrate.

This generated tissue blocked many, but not all, of the pores in the PTFE pouches (Supplementary Fig. S1; Supplementary Data are available online at www.liebertpub.com/tea). This blockage was especially noticeable in cross-sectional images, where less than 100 μm separated the opposite sides of the PTFE pores. H&E staining demonstrated that a highly cellular fibrous capsule was formed around most of the conduits, and recruited peritoneal cells were also observed to infiltrate and deposit matrix within the conduit wall (Fig. 2). Although images from only one representative animal/replicate are shown, the images for constructs grown within the other replicate were generally consistent. The H&E-stained cross sections of the tissue constructs show that the cell density was highest in the outer capsule and decreased inwardly throughout the thickness of the conduit wall. Quantitative image analysis of the distribution and quantity of DAPI-stained nuclei throughout the conduit wall demonstrated the same trend (Fig. 3A–C). Image analysis also indicated that the extent of cell infiltration was in general greater for conduits enclosed in the large-pore pouches compared to those in small-pore pouches. In addition, the extent of cell infiltration increased systematically for conduits with an increasing average fiber diameter ($p \leq 0.046$, for the hypothesis that the fiber diameter has an impact for all infiltration distances), especially for conduits within the large-pore pouch. The greatest cell infiltration occurred within the 22% w/v PCL conduits, where the recruited cells migrated ~200 μm into the conduit wall before a significant decrease in cellularity was noted. The opposite trend was observed with respect to the thickness of the fibrous capsule (Fig. 3D), with the 14.5% w/v PCL conduits within the large-pore pouch exhibiting significantly higher capsule thicknesses ($p = 0.026$, vs. 22% w/v PCL in the large-pore pouch). However, within the small-pore pouch, the constructs with very limited cell infiltration (i.e., 14.5% and 17% w/v PCL) exhibited more varied, but generally thicker fibrous capsules ($p = 0.043$, 14.5% w/v PCL in small-pore vs. large-pore pouch) (Fig. 3B, C).

The morphology of the cells recruited to the peritoneal constructs varied depending both on their position within the wall of the conduit and the specific condition (Fig. 2). Analysis of the nuclear area and aspect ratio from DAPI-stained images demonstrated that the nuclei were generally more elongated in the capsule compared to those within the

Table 1. Thickness and Average Fiber Diameters of Electrospun Conduits

Condition	*Wall thickness (μm)*	*Luminal fiber diameter (μm)*	*Outer fiber diameter (μm)*
14.5% PCL	439 ± 68	0.55 ± 0.3	0.62 ± 0.4
17.0% PCL	499 ± 100	1.5 ± 0.7	1.4 ± 0.7
22.0% PCL	462 ± 59	2.9 ± 0.6	1.9 ± 0.8

Table 2. The Degree and Direction of Orientation of Electrospun Conduits

Condition	*Luminal angular standard deviation (°)*	*Outer angular standard deviation (°)*	*Luminal difference in orientation (°)*	*Outer difference in orientation (°)*
14.5% PCL	53.7	56.4	35.6	36.9
17.0% PCL	40.6	60.6	6.29	11.7
22.0% PCL	52.5	51.6	0.09	85.1

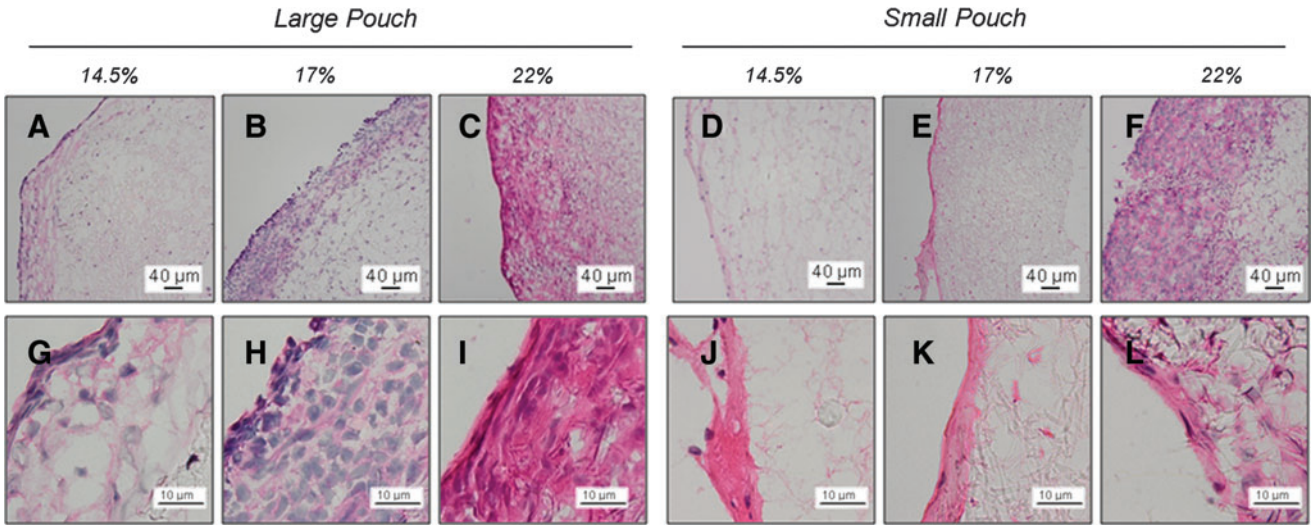

FIG. 2. Effect of average fiber diameter and pouch pore size on the morphology of recruited peritoneal cells and generated extracellular matrix (ECM). Shown are representative high- and low-magnification hematoxylin and eosin (H&E) images of 14.5% w/v **(A, D, G, J)**, 17% w/v **(B, E, H, K)**, and 22% w/v **(C, F, I, L)** that demonstrate differences in cell infiltration and cell morphology between different electrospinning concentrations. Cell nuclei are blue and cell cytoplasms and ECM (e.g., collagen) are pink. Conduits are shown after insertion in larger **(A–C, G–I)** or smaller pore pouches **(D–E, J–L)**, showing differences in cell morphology and generated matrix. The outer surface of the construct is on the left side. Color images available online at www.liebertpub.com/tea

electrospun conduit (Fig. 3E, F). In general, there were fewer and more rounded cells in the small-pore pouch. This difference in the nuclear aspect ratio was especially clear in the fibrous capsule ($p \leq 0.035$, small-pore vs. large-pore pouch). The exception appears to be the 22% w/v PCL conduits, which contain elongated cells similar to those inserted into large-pore pouches. For conduits within large-pore pouches, the nuclear aspect ratio generally decreased, and the area increased, with the decreasing solution concentration. This was independent of the distance within the conduit wall. The impact of the electrospun fiber diameter on the nuclear aspect ratio and area was less conclusive for conduits within small-pore pouches (not shown).

Impact on matrix content. The matrix content within constructs was determined both qualitatively with histological techniques and quantitatively with biochemical assays. Verhoff's-Van Gieson staining indicated that the recruited peritoneal cells produced a matrix rich in collagen (Fig. 4A–F). The collagen content was greater in the capsules, as indicated by the darker red or purple color present. However, some collagen deposition was also observed within the conduit wall. Systematic increases in collagen deposition within the conduit wall were observed with the increasing electrospun fiber diameter for constructs enclosed within the large-pore pouches, and were the greatest for the 22% w/v PCL condition. This corresponded to the electrospinning condition with the greatest cell infiltration, thinnest collagen-rich capsule (Fig. 4A–F), and the highest total cellularity ($p = 0.008$, 22% vs. 14.5% w/v PCL for all pouch pore sizes) (Fig. 4G). Total amounts of collagen, normalized to the luminal surface area, were not statistically different between conditions, although the collagen content appeared to be higher for constructs enclosed within the large-pore pouches ($p = 0.103$) (Fig. 4H). The elastin content in these constructs was limited, as indicated by both limited Verhoeff's Van Gieson staining and the Fastin assay. A few sporadic elastic fibers and amorphous elastin deposits were observed within the fibrous capsule (Fig. 4A–F). Less than 175 μg of elastin per cm^2 of the luminal surface area was present for all of the electrospinning conditions, as determined with the Fastin assay (Fig. 4I). All tissue constructs grown on PCL scaffolds contained comparable amounts of matrix elastin, regardless of the pouch type. Only the control PTFE conduits enclosed in the small pouch contained higher amounts of elastic matrix ($p = 0.003$, vs. 22% w/v PCL). The generated ECM also showed the presence of lipid droplets, especially within conduits contained in the small-pore pouches (Supplementary Fig. S2). Few lipid droplets, however, were present within conduits enclosed in the large-pore pouches. TEM images indicated that the ECM generated in all conduits contained significant amounts of ground substance (Fig. 4J), which stained positive for HA (Figs. 5A–C and 6A–C). Fibrin fibrils and collagen fibrils were also present, with minor variations in the quantity of individual matrix components between different experimental conditions (Fig. 4J). No elastic fibers and only a few amorphous elastin deposits were seen.

Impact on recruited peritoneal cell phenotype. TEM indicated the presence of several different cell types within the peritoneal constructs, regardless of the conduit type and pouch pore size (Supplementary Fig. S3). These include macrophages, with lysosomes and microvilli, and highly synthetic and extended fibroblastic cells, with several mitochondria and dilated cisterns of endoplasmic reticulum. Both cell types were found within the fibrous capsule. In addition, a mesothelial layer appeared to be present on the outer surface. Fewer cells and ECM were also found within the conduit wall.

Further characterizations of the cell phenotype revealed that groups of cells in the construct cross section stained

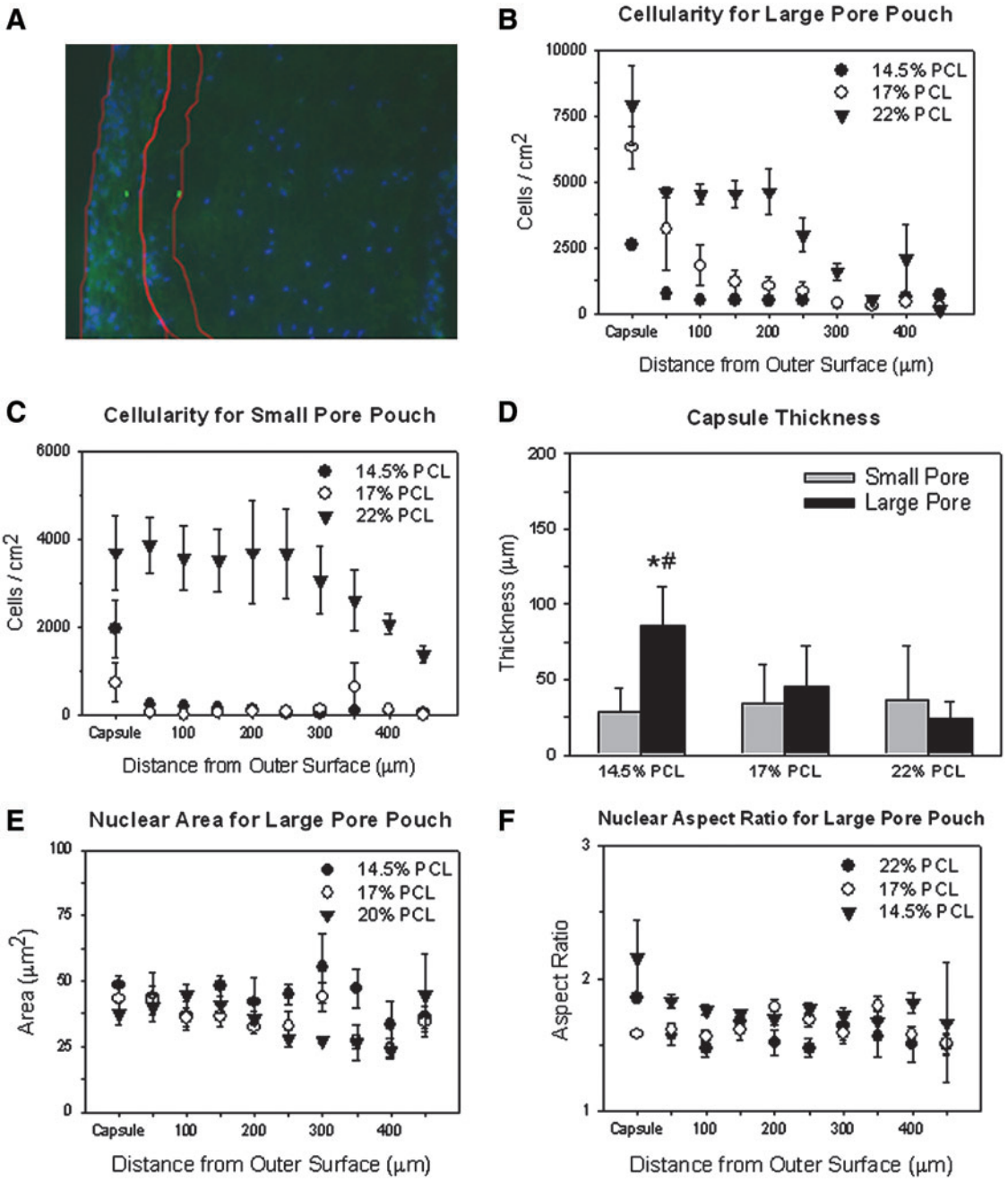

FIG. 3. Impact of electrospun fiber diameter and pouch pore size on peritoneal cell infiltration. Included is a large-pore pouch, 14.5% w/v PCL condition overlay image **(A)** with 4′,6-diamino-2-phenylindole dihydrochloride (DAPI)-stained nuclei (blue) and background autofluorescence (green) that shows the areas of interest created for the capsule and the first 50 μm within the electrospun fibers. The impact of electrospun condition on cellularity throughout the conduit wall (i.e., cell infiltration) was quantified for conduits within both large-pore **(B)** and small-pore **(C)** pouches. Results demonstrated greater cell infiltration with increasing electrospinning concentration. The capsule thickness for the different conditions were also compared **(D)**. The nuclear area **(E)** and aspect ratio **(F)** are shown for the large-pore pouches and demonstrate the change throughout the thickness of the conduit wall. The results are for $n = 4$ images/condition. *Statistical significance from the 22% w/v PCL condition; #significance from the small-pore pouch. Color images available online at www.liebertpub.com/tea

strongly for markers of myofibroblasts (i.e., α-SMA) and smooth muscle cells (i.e., SM22α and α-SMA) (Figs. 5D–I and 6D–I). The cells also stained for the general macrophage marker CD68 (Figs. 5J–L and 6J–L), although staining for the proinflammatory marker CD80 was negligible for most samples (not shown). Both the cells presenting SMC and macrophage markers were more prominent close to the outer surface of constructs (Fig. 5). More intense α-SMA staining was observed for conduits in large-pore pouches than for those in the small-pore pouches, with more α-SMA observed for the 22% and 17% w/v PCL conduits than for the 14.5% w/v PCL ones. In the small-pore pouches (Fig. 6), only the

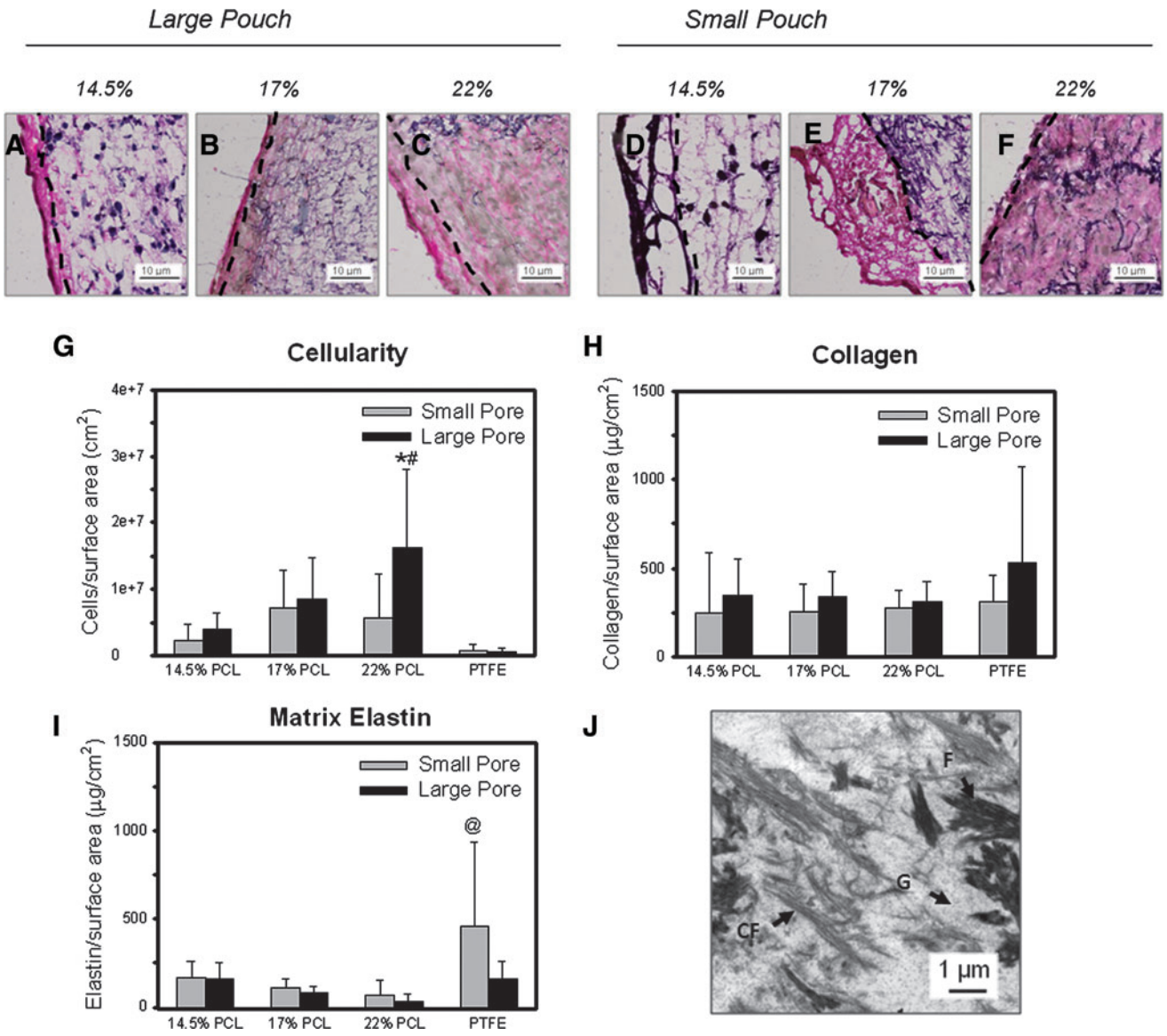

FIG. 4. Effect of average fiber diameter and pouch pore size on the composition and distribution of ECM components after 14 days in the peritoneal cavity. Shown are representative high-magnification images of modified Verhoff's stained 14.5% w/v **(A, D)**, 17% w/v **(B, E)**, and 22% w/v **(C, F)** constructs. Constructs are shown after insertion in larger **(A–C)** or smaller pore pouches **(D–F)**. Verhoff's Van Gieson stain shows collagen (pink/red), nuclei (light brown), elastic fibers (dark brown/black, as verified with an aorta-positive control), and PCL fibers and sporadic beads (dark purple). The outer surface of the construct is on the left side, and the start of the conduit walls are marked by dashed lines. Biochemical analysis was performed for recruited peritoneal cell densities as determined from DNA content **(G)**, collagen content determined with a hydroxyproline assay **(H)**, and matrix elastin content as determined with the Fastin® assay **(I)**. *Statistical significance from the small-pore pouch; #significance from the expanded PTFE (ePTFE) control and the smallest diameter 14.5% conduit; @significance from 22% PCL w/v for $n=6$ samples/condition and $n=2$ rats/condition. These figures show that significant collagen, but only a few elastic fibers are within the conduits. Detailed matrix structure was visualized using transmission electron microscopy **(J)**. C, collagen fibrils; F, fibrin fibrils; G, ground substance. Color images available online at www.liebertpub.com/tea

22% w/v PCL conduits showed any significant presence of α-SMA- and SM22α-positive cells. All constructs in the small-pore pouch stained positive for CD68, although with levels that varied with experimental condition. In both pouch pore size groups, constructs containing the largest diameter PCL fibers (i.e., 22% w/v PCL) exhibited more intense staining for CD68 than constructs containing the smaller diameter PCL fibers, especially the 14.5% w/v PCL constructs.

Mechanics of conduits and peritoneal constructs. Both nonimplanted electrospun PCL conduits and tissue constructs generated after 14 days in the peritoneal cavity, without enclosure within a pouch in this case, were mechanically tested at physiological conditions (Fig. 7). For nonimplanted PCL conduits, different stress–strain curves and breaking mechanisms were exhibited depending on the PCL concentration of the electrospinning solution

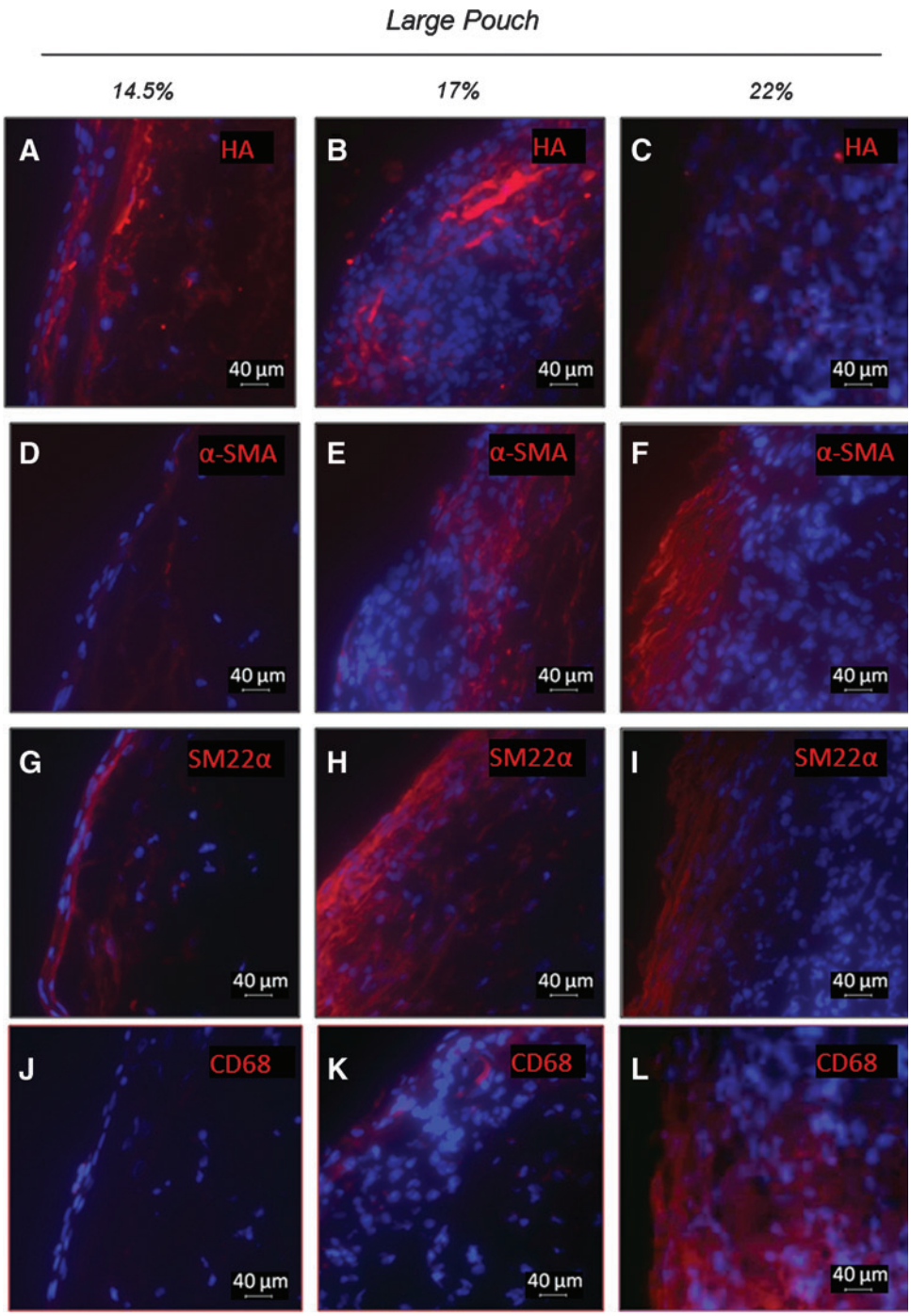

FIG. 5. Effect of average fiber diameter on the cell phenotype, cell morphology, and ECM components for conduits enclosed within large pore pouches. Shown are representative immunofluorescent images for hyaluronan (HA) **(A–C)** and myofibroblast, SMC, and macrophage markers. Markers include α-smooth muscle actin (α-SMA) **(D–F)**, SM22α **(G–I)**, and CD68 **(J–L)**. DAPI-stained nuclei are shown in blue. The outer surface of the construct is on the left side. Color images available online at www.liebertpub.com/tea

(Fig. 7A, B). The 20% w/v conduits had a long region of plastic deformation with groups of fibers breaking periodically, while the 14% w/v conduits exhibited a cleaner break. The stress–strain curve for the 17% w/v conduits showed characteristics between those observed for the 20% and 14% w/v conduits. After peritoneal insertion, the curve for the 14% w/v PCL constructs appeared similar to that of the nonimplanted conduits. However, the intraperitoneally implanted 20% and 17% w/v PCL constructs broke cleaner than identical, but nonimplanted conduits. These constructs also exhibited less of a plateau region before break. The tensile modulus for the 14% w/v PCL (i.e., 0.75 ± 0.14 MPa) was significantly lower than the 17% and 20% w/v PCL conduits (1.69 ± 0.45 and 1.75 ± 0.14 MPa, respectively) ($p < 0.001$) (Fig. 7C). Limited changes to the moduli were present in 20% w/v PCL conduits with intraperitoneal tissue generation, although there were differences for the 17% w/v PCL condition ($p = 0.005$, vs. conduit without tissue generation). The ultimate tensile strengths for all conduits (i.e., different electrospinning conditions) without implantation were similar (i.e., 1.1 MPa) (Fig. 7D). However, a significant increase was observed for the 17% w/v PCL condition with intraperitoneal implantation ($p < 0.001$).

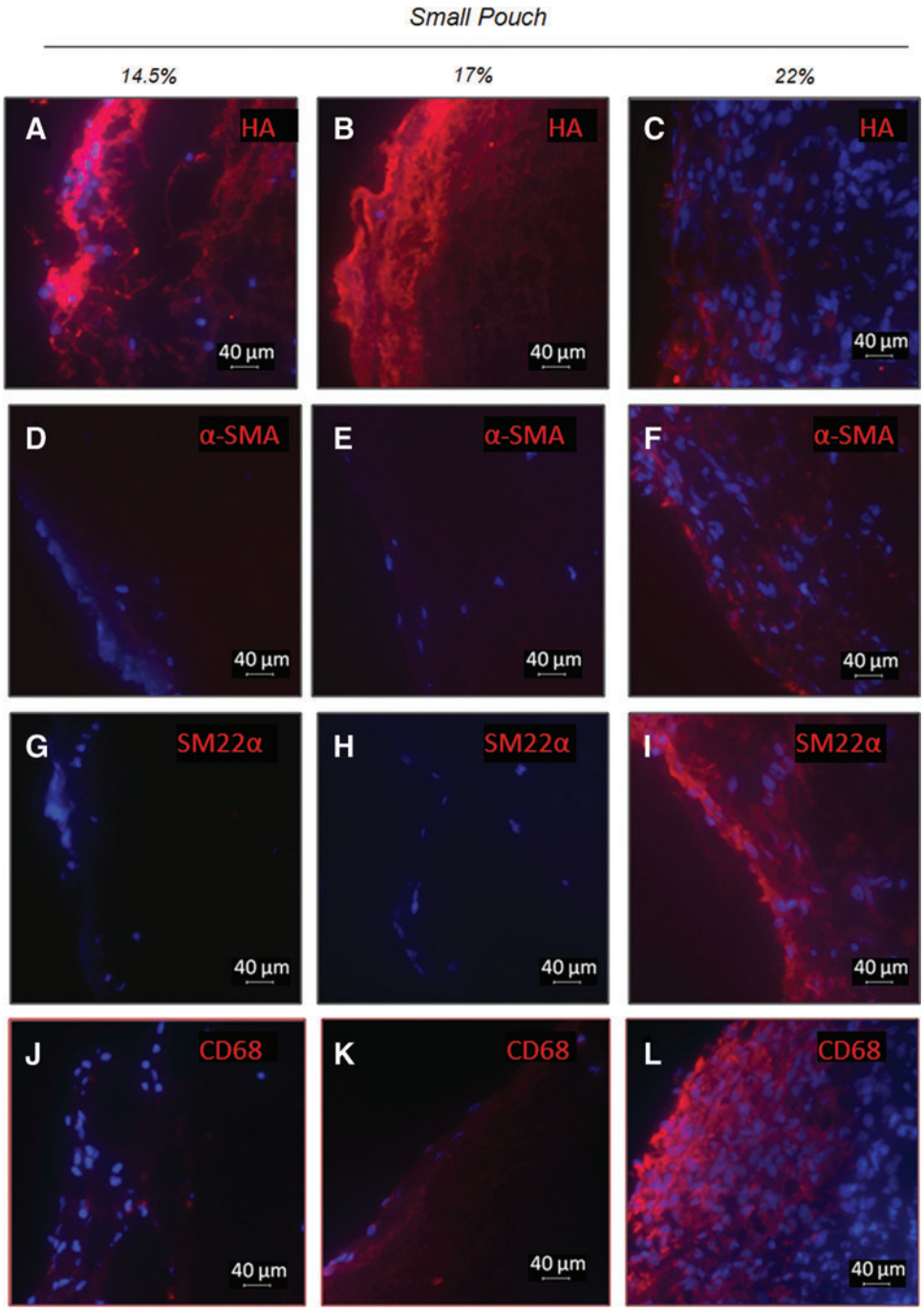

FIG. 6. Effect of average fiber diameter on the cell phenotype, cell morphology, and ECM components for conduits enclosed within small-pore pouches. Shown are representative immunofluorescent images for HA **(A–C)** and myofibroblast, SMC, and macrophage markers. Markers include α-SMA **(D–F)**, SM22α **(G–I)**, and CD68 **(J–L)**. DAPI-stained nuclei are shown in blue. The outer surface of the construct is on the left side. Color images available online at www.liebertpub.com/tea

Remodeling after intra-aortal grafting

Peritoneal constructs from 22% w/v PCL conduits were grafted into the abdominal aorta and removed after 6 weeks (Supplementary Fig. S4). The grafting surgery had a 50% success rate (i.e., 4/8), largely due to procedural and surgical complications. The rats were healthy and active through 6 weeks, even though the grafts, when explanted, were found to be significantly occluded. H&E staining demonstrated that cells were found throughout most of the thickness of the wall, but fewer cells were still found closer to the center. The H&E staining also demonstrated that matrix deposition colocalized with the cells. The lumen of the vessel was contracted, especially where more cells were present within the conduit wall, and filled with tissue. Large-scale remodeling of the construct occurred after grafting, with limited HA and α-SMA staining in the outer surface of the conduits, but significant staining for these markers within the lumen. No lipid droplets were present within the graft (not shown).

Discussion

It has previously been shown that small-diameter constructs with matrix organization similar to the vascular tissue can be produced by peritoneal cells around silicone tubes inserted into the peritoneal cavity.[17,19–21] However, there have been concerns within these studies (e.g., variability in

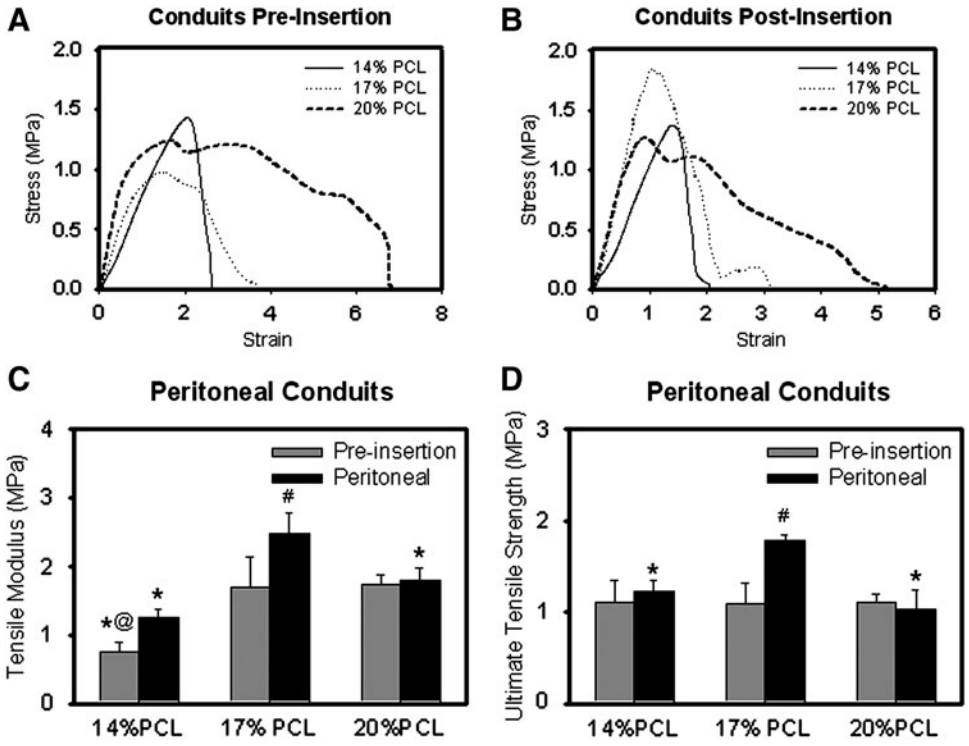

FIG. 7. Tensile properties of electrospun conduits/constructs. Shown are representative stress–strain curves for conduits both without implantation **(A)** and after 2 weeks of implantation **(B)** within the peritoneal cavity. The average tensile moduli **(C)** and ultimate tensile strength **(D)** for the different conditions are also shown for $n=6$ samples/condition preinsertion and $n=3$ samples/condition after 2 weeks in the peritoneal cavity. *Statistical significance from the 17% PCL condition; #significance change with 2 weeks in the peritoneal cavity; @significance from the 20% PCL condition.

the inflammatory response). An additional concern is the formation of tissue adhesions after implantation,[23] which we reduced in this study by enclosing the PCL conduits in a porous, PTFE pouch. We have also determined the impact of topographic features and the pore size of the enclosing pouch on the inflammatory response and elastic matrix deposition by recruited cells.

This study has demonstrated that the use of a pouch prevents the adhesion of the electrospun conduits to the surrounding tissue, but also that the pouch pore size significantly impacts the healing response. Many of the pores in the pouch were obstructed by the peritoneal cell-generated tissue after 2 weeks. For the small-pore pouches, it appeared that more of these pores were obstructed, likely limiting further convective transport of the peritoneal fluid and cells. This generally resulted in less cell infiltration, fewer, and less elongated cells, and limited ECM deposition within the wall of the conduit. The only exception was the largest diameter 22% w/v PCL conduits within the small-pore pouches. The reason for this exception is not known, although it is possible that the differing remodeling response for the 22% w/v PCL condition reduced the obstruction of the pores in the outer pouch.

A robust fibrous capsule was present around electrospun PCL conduits, but cells were also able to infiltrate into the conduit wall. This infiltration is necessary for a viable graft. The mixed population of cells within the constructs is evidence of a remodeling response. This population included myofibroblastic cells, macrophages (Figs. 5 and 6), and what appears to be an outer layer of mesothelial cells (Supplementary Fig. S3), similar to the cells that have been observed previously around silicone tubes implanted in the peritoneal cavity.[17,21] Interestingly, many of the cells within the construct stained positive for SM22α, similar to findings by Le *et al*.[21] SM22α is conventionally considered a SMC marker, but it has also been recently linked to myofibroblasts and nonmuscle cells transitioning to a SMC phenotype.[21,37,38] The presence of these ECM producing cells is likely necessary for continued tissue generation and maturation both in the peritoneal cavity and after grafting. Elongated macrophages (i.e., CD68-positive cells) were also present within these constructs; however, limited proinflammatory CD80 staining in these cells suggests that they also contribute to the healing response. While this study has not been designed to determine the origin of these differentiated cells, other studies have provided evidence for multiple sources.[39–41]

The recruited peritoneal cells deposited significant amounts of ECM within the construct, including collagen, fibrin (Fig. 4), and HA (Figs. 5 and 6), but limited amounts of elastic matrix. Collagen is a critical extracellular component of vascular tissues, but its abundant deposition is typical of a fibrotic tissue response.[42] The presence of fibrin indicates that inflammation is still continuing, and that the remodeling is delayed compared to normal wound-healing responses in the peritoneal cavity.[43] In addition, the limited production of elastic matrix in these constructs is consistent with previous attempts to generate a vascular-like tissue within the peritoneal cavity[17–19] and emphasizes the need to incorporate cues (e.g., elastogenic factors) into the conduits to stimulate elastic matrix generation.

Interestingly, the spatial distribution of individual ECM components within the electrospun conduit and in the surrounding capsule differed significantly. For example, the more elongated cells within the fibrous capsule were found to produce greater amounts of collagenous matrix than the more rounded cells within the conduit wall. This spatial heterogeneity in cell types and matrix deposition is likely partially due to differences in the microenvironment within the construct. These differences include the presence of porous, hydrolytically degradable PCL fibers within the conduit wall

compared to matrix metalloproteinase-degradable ECM surrounding cells in the fibrous capsule. Scaffolding chemistry has previously been shown to impact the phenotype of macrophages (e.g., proinflammatory M1 or prohealing M2),[44] and is likely a determinate of macrophage phenotype within our constructs. Surface topography or internal features to which cells can attach have also been shown to impact the macrophage phenotype. Madden *et al*.[27] demonstrated that macrophages exhibit more of a prohealing response (i.e., M2) when in a fibrous capsule compared to those within a scaffold with micro-spherical pores. In addition, they found a more prohealing response when the macrophages infiltrated within smaller (i.e., 30–40 μm) diameter pores compared to larger ones (e.g., 80 μm),[27] emphasizing the importance of phenotypic characterization of recruited cells.

In most of the constructs enclosed within small-pore pouches, significantly more lipid droplets were found in the fibrous capsule compared to constructs enclosed in large-pore pouches. Lipid accumulation in tissues is generally associated with the presence of macrophages, myofibroblasts, and synthetic SMCs in a pathological environment (e.g., foam cells in atherosclerotic legions).[45] Similarly, cells recruited to conduits within small-pore pouches stained predominately for macrophage markers (e.g., CD68), with the exception of the 22% w/v conduits. Myofibroblastic cells were not present, suggesting that the remodeling response within these constructs was either delayed or attenuated. The presence of extensive HA deposits in constructs within small-pore pouches further supports a delayed or more significant inflammatory response, since HA accumulation has been observed previously at sites of both vascular and peritoneal wound healing.[46] The presence of HA itself is not a concern since long-chain HA is known to play an important role in maintaining vascular integrity.[47] However, concerns include excess quantities of total HA and the presence of smaller fragments generated by enzymatic breakdown that are known to alter parenchymal cells behavior.[35,47]

Alternatively, the large-pore pouches promoted a more positive healing response for the conduits within (e.g., higher total cellularity, greater cell infiltration, more elongated cells, few lipid droplets, fewer HA deposits, and a significant number of α-SMA- and SM22α-positive cells). These results demonstrate the benefit of increasing the pouch pore size, as long as the surrounding peritoneal tissues are still unable to enter the pores. Patterns of tissue growth on/within conduits enclosed in the large-pore pouches were impacted by the electrospun fiber diameter. This dependence was less noticeable for conduits enclosed within small-pore pouches. Varying the diameter of the electrospun fibers changes both the topographic cues that guide cell spreading and alignment[30] and also the effective pore diameter of the scaffold.[25]

In the larger pore pouch conduits, the depth of cell infiltration into the conduit wall was the greatest (i.e., >200 μm) for conduits electrospun from 22% w/v PCL. These conduits contained the largest diameter fibers, and thus, the largest average pore sizes. The extent of cell infiltration into the conduit wall was likely also influenced by changes in scaffolding characteristics from the luminal to outer surfaces (e.g., a decrease in fiber diameter, changes in fiber packing, and a change in orientation). Similar changes in the electrospun scaffold structure have been observed by Pham *et al.*,[25] and may be attributed to differences in charge density and conductivity that occur as the electrospinning progresses. We also found other aspects of the remodeling response to be systematically impacted by the conduit average fiber diameter, with total cellularity, cell aspect ratio, and number of α-SMA-positive cells increasing with the increasing average fiber diameter. However, the capsule thickness and HA content decreased. Overall, these properties indicate that the larger 1.9-μm-diameter fibers elicit a better response from recruited peritoneal cells. However, the number of macrophages (i.e., CD68 staining) was also increased in constructs containing the largest diameter PCL fibers compared to those containing smaller fibers. Importantly, the lack of CD80, proinflammatory staining in the 22% w/v PCL constructs suggests that the elongated, activated macrophages are primarily of the prohealing M2 phenotype. These observations suggest that both smaller and larger diameters may provide different benefits for tissue generation, as has been shown previously with bone marrow stromal cells.[48] A balanced approach attempting both to replicate the size of native ECM components and to improve cell infiltration may be necessary to elicit an optimal tissue generation response (e.g., cell infiltration throughout the entire thickness of the conduit, robust ECM deposition, and the recruitment/differentiation of peritoneal cells to SMCs).

The peritoneal constructs demonstrated tensile moduli comparable to tissue-free electrospun PCL meshes[29] and also to human coronary arteries (i.e., ~1.8 MPa).[28] Modest increases in tensile modulus and ultimate tensile strength were observed compared to nonimplanted PCL conduits, likely due to accumulation of collagenous matrix. The collagenous matrix may have helped to hold individual fibers together (e.g., essentially creating more fiber–fiber intersection points).[49] This may have enabled the fibers to break more cleanly as a group, instead of discretely in steps, like the 20% w/v PCL conduits without extra tissue. After grafting the constructs autologously into the aorta, the constructs were found to remodel (e.g., cells infiltrated further into the conduit wall and the most intense staining for α-SMA and HA transitioned from the outer surface to along the lumen of the vessel). However, the intra-aortally transplanted grafts were occluded after 6 weeks in the rats. This occlusion appeared to occur due to initial constriction of the vessel (e.g., from suturing), intimal hyperplasia, and thrombosis arising from the lack of a functional endothelium. Poor luminal endothelialization is a common problem with vascular grafts and has been addressed through multiple techniques, including adding a vascular endothelial growth factor to the lumen of a graft[50] and seeding the lumen of electrospun conduits with endothelial cells.[22,51]

An additional, yet unaddressed requirement for vascular grafts is the production of a significant quantity and quality of elastic matrix. This study has established that elastic matrix is produced by peritoneal cells recruited to an electrospun PCL mesh, but also that further elastic matrix production is required. One of the major concerns with these constructs is that their stress–strain curve exhibits a limited toe-region, and thus, limited elastic behavior, unlike elastic lamellae in native vessels.[52] The elastic matrix generation is even more important for long-term patency, especially when the scaffold material degrades. These concerns highlight the importance of combining the peritoneal cavity model with

other strategies that have been shown to improve elastic matrix production[13,14] and also potentially increasing the duration of time in the peritoneal cavity to allow further differentiation of the recruited cells.[18,20,21]

Conclusions

This study shows that peritoneal cells recruited onto electrospun conduits in the peritoneal cavity give rise to several cell types, including SMCs/myofibroblasts, mesothelial cells, and macrophages. A functional endothelium was not generated, as was found to result in graft occlusion when implanted intra-aortally. The cells generated components of the vascular ECM, including collagen and HA, but few elastic fibers. Since these elastic fibers are a critical component of the vascular tissue, this study highlights the need for additional scaffold-based stimuli to promote elastogenesis. The study additionally shows that both pore sizes of conduit-enclosing pouches and microenvironmental cues (i.e., electrospun average fiber diameters) critically influence cell infiltration, depth of cell penetration within the conduit wall, and tissue remodeling within the conduits. Overall, this study demonstrates the importance of the microenvironment surrounding the peritoneal cells, but also suggests that longer peritoneal implantation times may be required to allow greater tissue remodeling and maturation.

Acknowledgments

This study was supported by NIH Grants from the National Heart, Lung, and Blood Institute (HL092051-01A1 and HL092051-01S) and the National Institute of Biomedical Imaging and Bioengineering (EB006078-01A1) awarded to Ramamurthi A. This project was also funded by an NIH postdoctoral fellowship (F32HL108548-01A1) awarded to C.A. Bashur.

Disclosure Statement

No competing financial interests exist.

References

1. McGill, H.C., Jr., McMahan, C.A., Herderick, E.E., Malcom, G.T., Tracy, R.E., and Strong, J.P. Origin of atherosclerosis in childhood and adolescence. Am J Clin Nutr **72,** 1307S, 2000.
2. Lloyd-Jones, D., Adams, R., Carnethon, M., De Simone, G., Ferguson, T.B., Flegal, K., Ford, E., Furie, K., Go, A., Greenlund, K., Haase, N., Hailpern, S., Ho, M., Howard, V., Kissela, B., Kittner, S., Lackland, D., Lisabeth, L., Marelli, A., McDermott, M., Meigs, J., Mozaffarian, D., Nichol, G., O'Donnell, C., Roger, V., Rosamond, W., Sacco, R., Sorlie, P., Stafford, R., Steinberger, J., Thom, T., Wasserthiel-Smoller, S., Wong, N., Wylie-Rosett, J., and Hong, Y. Heart disease and stroke statistics—2009 update: a report from the American Heart Association Statistics Committee and Stroke Statistics Subcommittee. Circulation **119,** e21, 2009.
3. Klinkert, P., Post, P.N., Breslau, P.J., and van Bockel, J.H. Saphenous vein versus PTFE for above-knee femoropopliteal bypass. A review of the literature. Eur J Vasc Endovasc Surg **27,** 357, 2004.
4. Chlupac, J., Filova, E., and Bacakova, L. Blood vessel replacement: 50 years of development and tissue engineering paradigms in vascular surgery. Physiol Res **58 Suppl 2,** S119, 2009.
5. Kielty, C.M., Stephan, S., Sherratt, M.J., Williamson, M., and Shuttleworth, C.A. Applying elastic fibre biology in vascular tissue engineering. Philos Trans R Soc Lond B Biol Sci **362,** 1293, 2007.
6. Shin'oka, T., Matsumura, G., Hibino, N., Naito, Y., Watanabe, M., Konuma, T., Sakamoto, T., Nagatsu, M., and Kurosawa, H. Midterm clinical result of tissue-engineered vascular autografts seeded with autologous bone marrow cells. J Thorac Cardiovasc Surg **129,** 1330, 2005.
7. L'Heureux, N., Dusserre, N., Konig, G., Victor, B., Keire, P., Wight, T.N., Chronos, N.A., Kyles, A.E., Gregory, C.R., Hoyt, G., Robbins, R.C., and McAllister, T.N. Human tissue-engineered blood vessels for adult arterial revascularization. Nat Med **12,** 361, 2006.
8. Konig, G., McAllister, T.N., Dusserre, N., Garrido, S.A., Iyican, C., Marini, A., Fiorillo, A., Avila, H., Wystrychowski, W., Zagalski, K., Maruszewski, M., Jones, A.L., Cierpka, L., de la Fuente, L.M., and L'Heureux, N. Mechanical properties of completely autologous human tissue engineered blood vessels compared to human saphenous vein and mammary artery. Biomaterials **30,** 1542, 2009.
9. Bashur, C.A., Venkataraman, L., and Ramamurthi, A. Tissue engineering and regenerative strategies to replicate biocomplexity of vascular elastic matrix assembly. Tissue Eng Part B Rev 2012 [Epub ahead of print]; DOI: 10.1089/ten.teb.2011.0521. Available at www.ncbi.nlm.nih.gov/pubmed/22224468.
10. Gong, Z., and Niklason, L.E. Small-diameter human vessel wall engineered from bone marrow-derived mesenchymal stem cells (hMSCs). FASEB J **22,** 1635, 2008.
11. Kielty, C.M., Sherratt, M.J., and Shuttleworth, C.A. Elastic fibres. J Cell Sci **115,** 2817, 2002.
12. Fornieri, C., Quaglino, D., Jr., and Mori, G. Role of the extracellular matrix in age-related modifications of the rat aorta. Ultrastructural, morphometric, and enzymatic evaluations. Arterioscler Thromb **12,** 1008, 1992.
13. Bashur, C.A., and Ramamurthi, A. Aligned electrospun scaffolds and elastogenic factors for vascular cell-mediated elastic matrix assembly. J Tissue Eng Regen Med 2011 [Epub ahead of print]; DOI: 10.1002/term.470. Available at www.ncbi.nlm.nih.gov/pubmed/21953981
14. Kothapalli, C.R., Taylor, P.M., Smolenski, R.T., Yacoub, M.H., and Ramamurthi, A. Transforming growth factor beta 1 and hyaluronan oligomers synergistically enhance elastin matrix regeneration by vascular smooth muscle cells. Tissue Eng Part A **15,** 501, 2009.
15. Johnson, D.J., Robson, P., Hew, Y., and Keeley, F.W. Decreased elastin synthesis in normal development and in long-term aortic organ and cell cultures is related to rapid and selective destabilization of mRNA for elastin. Circ Res **77,** 1107, 1995.
16. McMahon, M.P., Faris, B., Wolfe, B.L., Brown, K.E., Pratt, C.A., Toselli, P., and Franzblau, C. Aging effects on the elastin composition in the extracellular matrix of cultured rat aortic smooth muscle cells. In Vitro Cell Dev Biol **21,** 674, 1985.
17. Campbell, J.H., Efendy, J.L., and Campbell, G.R. Novel vascular graft grown within recipient's own peritoneal cavity. Circ Res **85,** 1173, 1999.
18. Song, L., Wang, L., Shah, P.K., Chaux, A., and Sharifi, B.G. Bioengineered vascular graft grown in the mouse peritoneal cavity. J Vasc Surg **52,** 994, 2010.

19. Chue, W.L., Campbell, G.R., Caplice, N., Muhammed, A., Berry, C.L., Thomas, A.C., Bennett, M.B., and Campbell, J.H. Dog peritoneal and pleural cavities as bioreactors to grow autologous vascular grafts. J Vasc Surg **39,** 859, 2004.
20. Campbell, J.H., Efendy, J.L., Han, C., Girjes, A.A., and Campbell, G.R. Haemopoietic origin of myofibroblasts formed in the peritoneal cavity in response to a foreign body. J Vasc Res **37,** 364, 2000.
21. Le, S.J., Gongora, M., Zhang, B., Grimmond, S., Campbell, G.R., Campbell, J.H., and Rolfe, B.E. Gene expression profile of the fibrotic response in the peritoneal cavity. Differentiation **79,** 232, 2010.
22. Zhang, Z.X., Xi, T.F., Wang, Y.J., Chen, X.S., Zhang, J., Wang, C.R., Gu, Y.Q., Chen, L., Li, J.X., and Chen, B. *In vitro* study of endothelial cells lining vascular grafts grown within the recipient's peritoneal cavity. Tissue Eng Part A **14,** 1109, 2008.
23. Cao, Y., Zhang, B., Croll, T., Rolfe, B.E., Campbell, J.H., Campbell, G.R., Martin, D., and Cooper-White, J.J. Engineering tissue tubes using novel multilayered scaffolds in the rat peritoneal cavity. J Biomed Mater Res A **87,** 719, 2008.
24. Rossi, A., Pasqui, D., Barbucci, R., Gerli, R., and Weber, E. The topography of microstructured surfaces differently affects fibrillin deposition by blood and lymphatic endothelial cells in culture. Tissue Eng Part A **15,** 525, 2009.
25. Pham, Q.P., Sharma, U., and Mikos, A.G. Electrospun poly(epsilon-caprolactone) microfiber and multilayer nanofiber/microfiber scaffolds: characterization of scaffolds and measurement of cellular infiltration. Biomacromolecules **7,** 2796, 2006.
26. Baker, B.M., Gee, A.O., Metter, R.B., Nathan, A.S., Marklein, R.A., Burdick, J.A., and Mauck, R.L. The potential to improve cell infiltration in composite fiber-aligned electrospun scaffolds by the selective removal of sacrificial fibers. Biomaterials **29,** 2348, 2008.
27. Madden, L.R., Mortisen, D.J., Sussman, E.M., Dupras, S.K., Fugate, J.A., Cuy, J.L., Hauch, K.D., Laflamme, M.A., Murry, C.E., and Ratner, B.D. Proangiogenic scaffolds as functional templates for cardiac tissue engineering. Proc Natl Acad Sci U S A **107,** 15211, 2010.
28. Holzapfel, G.A., Sommer, G., Gasser, C.T., and Regitnig, P. Determination of layer-specific mechanical properties of human coronary arteries with nonatherosclerotic intimal thickening and related constitutive modeling. Am J Physiol Heart Circ Physiol **289,** H2048, 2005.
29. Vaz, C.M., van Tuijl, S., Bouten, C.V., and Baaijens, F.P. Design of scaffolds for blood vessel tissue engineering using a multi-layering electrospinning technique. Acta Biomater **1,** 575, 2005.
30. Bashur, C.A., Dahlgren, L.A., and Goldstein, A.S. Effect of fiber diameter and orientation on fibroblast morphology and proliferation on electrospun poly(D,L-lactic-co-glycolic acid) meshes. Biomaterials **27,** 5681, 2006.
31. Soffer, L., Wang, X., Zhang, X., Kluge, J., Dorfmann, L., Kaplan, D.L., and Leisk, G. Silk-based electrospun tubular scaffolds for tissue-engineered vascular grafts. J Biomater Sci Polym Ed **19,** 653, 2008.
32. Hoenig, M.R., Campbell, G.R., Rolfe, B.E., and Campbell, J.H. Tissue-engineered blood vessels: alternative to autologous grafts? Arterioscler Thromb Vasc Biol **25,** 1128, 2005.
33. Richard, M.N., Deniset, J.F., Kneesh, A.L., Blackwood, D., and Pierce, G.N. Mechanical stretching stimulates smooth muscle cell growth, nuclear protein import, and nuclear pore expression through mitogen-activated protein kinase activation. J Biol Chem **282,** 23081, 2007.
34. Labarca, C., and Paigen, K. A simple, rapid, and sensitive DNA assay procedure. Anal Biochem **102,** 344, 1980.
35. Joddar, B., and Ramamurthi, A. Fragment size- and dose-specific effects of hyaluronan on matrix synthesis by vascular smooth muscle cells. Biomaterials **27,** 2994, 2006.
36. Stegemann, H., and Stalder, K. Determination of hydroxyproline. Clin Chim Acta **18,** 267, 1967.
37. Sartore, S., Chiavegato, A., Faggin, E., Franch, R., Puato, M., Ausoni, S., and Pauletto, P. Contribution of adventitial fibroblasts to neointima formation and vascular remodeling: from innocent bystander to active participant. Circ Res **89,** 1111, 2001.
38. Faggin, E., Puato, M., Zardo, L., Franch, R., Millino, C., Sarinella, F., Pauletto, P., Sartore, S., and Chiavegato, A. Smooth muscle-specific SM22 protein is expressed in the adventitial cells of balloon-injured rabbit carotid artery. Arterioscler Thromb Vasc Biol **19,** 1393, 1999.
39. Herrick, S.E., and Mutsaers, S.E. Mesothelial progenitor cells and their potential in tissue engineering. Int J Biochem Cell Biol **36,** 621, 2004.
40. Abe, R., Donnelly, S.C., Peng, T., Bucala, R., and Metz, C.N. Peripheral blood fibrocytes: differentiation pathway and migration to wound sites. J Immunol **166,** 7556, 2001.
41. Guo, Y., Lubbert, M., and Engelhardt, M. CD34- hematopoietic stem cells: current concepts and controversies. Stem Cells **21,** 15, 2003.
42. Kim, L., Kim do, K., Yang, W.I., Shin, D.H., Jung, I.M., Park, H.K., and Chang, B.C. Overexpression of transforming growth factor-beta 1 in the valvular fibrosis of chronic rheumatic heart disease. J Korean Med Sci **23,** 41, 2008.
43. Cheong, Y.C., Laird, S.M., Li, T.C., Shelton, J.B., Ledger, W.L., and Cooke, I.D. Peritoneal healing and adhesion formation/reformation. Hum Reprod Update **7,** 556, 2001.
44. Badylak, S.F., Valentin, J.E., Ravindra, A.K., McCabe, G.P., and Stewart-Akers, A.M. Macrophage phenotype as a determinant of biologic scaffold remodeling. Tissue Eng Part A **14,** 1835, 2008.
45. Olsen, A.L., Bloomer, S.A., Chan, E.P., Gaca, M.D., Georges, P.C., Sackey, B., Uemura, M., Janmey, P.A., and Wells, R.G. Hepatic stellate cells require a stiff environment for myofibroblastic differentiation. Am J Physiol Gastrointest Liver Physiol **301,** G110, 2011.
46. Toole, B.P., Wight, T.N., and Tammi, M.I. Hyaluronan-cell interactions in cancer and vascular disease. J Biol Chem **277,** 4593, 2002.
47. Lennon, F.E., and Singleton, P.A. Hyaluronan regulation of vascular integrity. Am J Cardiovasc Dis **1,** 200, 2011.
48. Bashur, C.A., Shaffer, R.D., Dahlgren, L.A., Guelcher, S.A., and Goldstein, A.S. Effect of fiber diameter and alignment of electrospun polyurethane meshes on mesenchymal progenitor cells. Tissue Eng Part A **15,** 2435, 2009.
49. Stylianopoulos, T., Bashur, C.A., Goldstein, A.S., Guelcher, S.A., and Barocas, V.H. Computational predictions of the tensile properties of electrospun fibre meshes: effect of fibre diameter and fibre orientation. J Mech Behav Biomed Mater **1,** 326, 2008.
50. Zhou, M., Liu, Z., Wei, Z., Liu, C., Qiao, T., Ran, F., Bai, Y., Jiang, X., and Ding, Y. Development and validation of small-diameter vascular tissue from a decellularized scaffold coated with heparin and vascular endothelial growth factor. Artif Organs **33,** 230, 2009.

51. Tillman, B.W., Yazdani, S.K., Lee, S.J., Geary, R.L., Atala, A., and Yoo, J.J. The *in vivo* stability of electrospun polycaprolactone-collagen scaffolds in vascular reconstruction. Biomaterials **30,** 583, 2009.
52. Armentano, R.L., Levenson, J., Barra, J.G., Fischer, E.I., Breitbart, G.J., Pichel, R.H., and Simon, A. Assessment of elastin and collagen contribution to aortic elasticity in conscious dogs. Am J Physiol **260,** H1870, 1991.

Address correspondence to:
Anand Ramamurthi, PhD
Department of Biomedical Engineering
Cleveland Clinic
9500 Euclid Ave./ND20
Cleveland, OH 44195

E-mail: ramamua@ccf.org

Received: May 18, 2012
Accepted: October 16, 2012
Online Publication Date: November 29, 2012